Electronic Research Archive

ERA, 32(2): 962–978.
DOI: 10.3934/era.2024047
Received: 23 November 2023
Revised: 24 December 2023
Accepted: 04 January 2024
Published: 18 January 2024

http://www.aimspress.com/journal/ERA

Theory article

Oblique impact dynamic analysis of wedge friction damper with Dankowicz dynamic friction

Yanlong Zhang[1,*], Rui Zhang[1,*] and Li Wang[2]

[1] School of Mechatronic Engineering, Lanzhou Jiaotong University, Lanzhou 730070, China
[2] School of Information Engineering, Lanzhou City University, Lanzhou 730070, China

* **Correspondence:** Email: zhangyl@mail.lzjtu.cn, 3281083283@qq.com.

Abstract: Aiming at the wedge friction damper for freight train bogie, considering Dankowicz dynamic friction, the mechanical model of a three-degree-of-freedom inclined impact vibration system with gap and dynamic friction, is simplified. The mechanical model of the system is established, the motion equation of the system is obtained, and the motion state and conditions of the system are analyzed. The Poincare map is constructed by selecting a fixed collision section, and the response of the system is solved by the fourth-order Runge-Kutta numerical method with variable step size. The transition process of the system motion and the phenomenon of sticking and chatter are analyzed by numerical simulation when the external excitation frequency changes. The results show that: 1) Under certain parameters, with the change of excitation frequency, the system undergoes periodic doubling bifurcation, inverse periodic doubling bifurcation, Grazing bifurcation and Hopf bifurcation, and there is a "periodic bubble" phenomenon in the system motion. When the system excitation frequency is between 3.35–3.55, 4.425–6.12, and 7.34–7.758, the system motion has chatter and sticking phenomena; when the system excitation frequency is between 1.75–3.24 and 3.92–4.425, the sticking phenomenon disappears, and only the chatter phenomenon exists. 2) When other parameters remain unchanged, and the mass ratio decreases from 1.15 to 0.85, nonlinear dynamic phenomena such as the transition between periodic bubbles and chaotic bubbles will be found. In this paper, the bifurcation and chaos characteristics of the impact vibration system of the wedge friction damper are studied, and the rich friction-induced vibration forms such as chatter and sticking are revealed, which provides a reference for improving the stability of vehicle operation and the selection of parameters in vehicle vibration reduction design in engineering practice.

Keywords: wedge friction damper; oblique collision; dynamic friction; bifurcation; sticking; chatter

1. Introduction

Contact collision is a common phenomenon in engineering practice. With the deepening of scholars' research, the frontal collision model cannot describe the oblique collision system with tilt angle more accurately. Therefore, the oblique collision system with collision angle should be studied in depth. In addition, friction is inevitable in the process of oblique collision. The vibration caused by friction affects the stability of the system, accelerates the wear failure of the parts, and has potential safety hazards. Duan and Ding [1] discussed the influence of collision parameters such as mass clearance and contact surface inclination on the vibration reduction effect of turbine shroud blade group system through phase trajectory diagram, bifurcation diagram, and Poincare section diagram. Ling et al. [2] established a mechanical model of oblique collision between freight cars and trains at railway crossings and studied the dynamic response and derailment mechanism of trains in this scenario using the multi-body dynamics method. Dong and Ding [3] established the oblique collision model and equation of the whole ring bladed disk system with a shroud and analyzed the dynamic response of the blade when the gap between the shrouds and the stiffness of the blade are misaligned. In [4–8], the mechanical model with oblique collision was simplified for the actual engineering model, and the dynamic behaviors such as oblique collision motion and bifurcation phenomenon of the system in engineering practice were studied. Considering the dynamic friction of LuGre, Liu et al. [9] established a friction model of blade crown collision, and studied the bifurcation characteristics of contact collision and friction motion of shrouded blades. For the single-degree-of-freedom system with improved LuGre dynamic friction, Saha et al. [10] analyzed the sticking phenomenon of the system through the phase diagram, and compared and analyzed the dynamic characteristics of the system under LuGre and improved LuGre dynamic friction. Zhang et al. [11] introduced the Dankowicz dynamic friction model into the single-degree-of-freedom vibration system, analyzed the motion state and judgment conditions, and studied the friction-induced system vibration and the dynamic behavior of the system under the influence of two parameters.

The wedge friction damper is one of the key components of the three-piece bogie [12], which has an important influence on the dynamic performance of the vehicle. Li [13] analyzed the vibration characteristics of a 100 t heavy-duty truck with a wedge friction damper and found the influence of the relative friction coefficient of the damping system on the stability of the truck. Based on vehicle system dynamics, Song et al. [14] used SIMPACK software to establish a nonlinear dynamic model of six-axle flat car and analyzed the influence and variation of different friction angles on the dynamics of three-axle bogie. Li et al. [12] used SIMPACK software to establish the mechanical model of the wedge friction damper and analyzed the spatial force and vibration reduction performance of the model. Liu [15] introduced the structure of wedge friction damper for three-piece bogie of freight train bogie, analyzed the design value of the relative friction coefficient of the product, and gave the value suggestion.

On the basis of [12–15], aiming at the wedge friction damper for freight train bogie, in order to be closer to the actual working conditions and describe the friction-induced vibration characteristics more comprehensively, the dynamic friction between the wedge and the side frame is considered, and a three-degree-of-freedom oblique collision vibration system with Dankowicz dynamic friction and gap

is simplified. The motion equation of the system is established, and the motion state of the system and its judgment conditions are analyzed. Based on C language programming and variable step size fourth-order Runge-Kutta algorithm, the numerical simulation analyzes the evolution process of the system motion and the frequency range of the viscous and flutter phenomena when the external excitation frequency changes, which can provide a certain reference for the selection of system structure parameters in engineering practice.

2. Modeling of the wedge friction damper system

The following Figure 1 shows a wedge friction damper. The numbers 1–9 in the figure are bolster, right wedge, left wedge, intermediate bolster spring, right bolster spring, left bolster spring, right sub-wedge spring, left sub-wedge spring, and side frame.

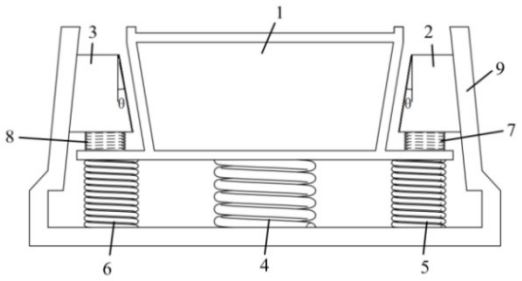

Figure 1. Wedge friction damper.

In order to be closer to the actual working conditions and consider the influence of vibration reduction and lubrication, the bolster 1 is simplified into a mass block M_1; the wedge blocks 2 and 3 are simplified into block M_2 and block M_3, respectively. The damping spring 7 and 8 connected by the wedge block 2 and 3 are simplified to the nonlinear spring K_2 and the nonlinear spring K_3, respectively. The lubricating oil between the bolster 1 and the wedge block is simplified as a nonlinear damping sum C_2 and C_3, respectively. The bolster spring 4, 5, 6 is simplified into a nonlinear spring K_1; the air damping of the bolster is simplified to linear damping C_1; the contact surfaces between the wedge block 2, 3 and the side frame 9 are A and B surfaces, and there is sliding friction force between the contact surfaces; and a dynamic model of the wedge damper with dynamic friction and gap is obtained, as shown in Figure 2.

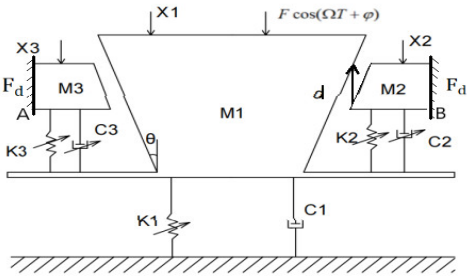

Figure 2. Dynamic model of wedge friction damper with friction.

Between two adjacent collisions, the differential equation of system motion is:

$$\begin{cases} M_1\ddot{X}_1 + F_1 - F_2 - F_3 - \bar{F}_2 - \bar{F}_3 + C_1\dot{X}_1 = F\,cos(\Omega T + \varphi) \\ M_2\ddot{X}_2 + F_2 + \bar{F}_2 = F_d \\ M_3\ddot{X}_3 + F_3 + \bar{F}_3 = F_d \end{cases} \tag{1}$$

In Eq (1): F_d is the dynamic friction generated between the contact surface of the bolster 1 and the side frame 9 during the movement of the wedge friction damper; F_i is the nonlinear spring force of the damping spring K_i, where E is a small parameter; $\bar{F}_i$ is a nonlinear damping force [16].

$$F_i = K_iX_i + EK_iX_i^3 \tag{2}$$

In Eq (2), $i = 1, 2, 3$

$$\bar{F}_i = C_i[1 + Hsign(\dot{X}_i - \dot{X}_1)](\dot{X}_i - \dot{X}_1)^{\frac{1}{3}} \tag{3}$$

In Eq (3), $i = 2, 3$, H is the asymmetry coefficient, which represents the unequal degree of damping force between the recovery stroke and the compression stroke of the shock absorber, where

$$\text{sign}(\dot{X}_i - \dot{X}_1) = \begin{cases} 1, & \dot{X}_i - \dot{X}_1 > 0 \\ -1, & \dot{X}_i - \dot{X}_1 < 0 \end{cases} \tag{4}$$

Select the initial displacement $\mathrm{L}_1 = \mathrm{x}_1(0)$ as the length scale, construct the time scale $T_1 = \sqrt{\frac{M_1}{K_1}}$, and take the dimensionless parameter as:

$$m_2 = \frac{M_2}{M_1},\ m_3 = \frac{M_3}{M_1},\ k_1 = \frac{K_1T_1^2}{M_1},\ k_2 = \frac{K_2T_1^2}{M_1},\ k_3 = \frac{K_3T_1^2}{M_1},\ \xi_1 = \frac{C_1T_1}{M_1},\ \xi_2 = \frac{C_2T_1^{\frac{5}{3}}}{M_1L_1^{\frac{2}{3}}},\ \xi_3 = \frac{\mathrm{C_3T_1^{\frac{5}{3}}}}{M_1\mathrm{L_1^{\frac{2}{3}}}},\ \eta = \frac{L_1}{T_1}H,$$

$$f = \frac{F\,T_1^2}{M_1L_1},\ f_d = \frac{F_d\,T_1^2}{M_1L_1},\ \omega = \Omega T_1,\ \varepsilon = EL_1^2,\ t = \frac{T}{T_1},\ x_i = \frac{X_i}{L_1},\ i = 1, 2, 3.$$

Substituting the above dimensionless parameters into Eq (1), the dimensionless equation of the system motion can be obtained:

$$\begin{cases} \ddot{x}_1 = f\,cos(wt + \varphi) - \xi_1\dot{x}_1 - k_1x_1 - \varepsilon k_1x_1^3 + k_2x_2 + \varepsilon k_2x_2^3 + k_3x_3 + \varepsilon k_3x_3^3 \\ +\xi_2[1 + \eta\,sgn(\dot{x}_2 - \dot{x}_1)](\dot{x}_2 - \dot{x}_1)^{1/3} + \xi_3[1 + \eta\,sgn(\dot{x}_3 - \dot{x}_1)](\dot{x}_3 - \dot{x}_1)^{1/3} \\ \ddot{x}_2 = \frac{1}{m_2}[-k_2x_2 - \varepsilon k_2x_2^3 + f_d - \xi_2[1 + \eta\,sgn(\dot{x}_2 - \dot{x}_1)](\dot{x}_2 - \dot{x}_1)^{1/3}] \\ \ddot{x}_3 = \frac{1}{m_3}[-k_3x_3 - \varepsilon k_3x_3^3 + f_d - \xi_3[1 + \eta\,sgn(\dot{x}_3 - \dot{x}_1)](\dot{x}_3 - \dot{x}_1)^{1/3}] \end{cases} \tag{5}$$

The dimensionless expression Eq (6) of Dankowicz dynamic friction model is [17]:

$$f_d = f_r(\mu e^{-y/\sigma}\frac{z}{\delta} + \alpha_1{v_r}^2 sgn(v_r)(1 - \frac{y}{y_\infty})e^{-y/\sigma}) + \sigma_1\dot{z} \tag{6}$$

In Eq (6), f_r represents the normal total load on the contact surface, μ represents the friction

coefficient, σ represents the standard deviation of the roughness height, δ represents the maximum allowable asperity deformation, $v_r = \dot{x}_1 - \dot{x}_i$ represents the relative slip velocity between mass 1 and mass 2 or mass 3, y_∞ represents the separation distance from the radius of the asperity to the normal direction, σ_1 is the bristle damping, α_1 is an ordinary parameter, and $\dot{z}$ is the internal damping term. The evolution of the internal variable z of the dynamic friction model is dominated by Eq (7):

$$\dot{z} = v_r\left(1 - \frac{z}{\delta} sgn(v_r)\right) \tag{7}$$

In Eq (7), for $v_r > 0$, z tends to δ; for $v_r < 0$, z tends to $-\delta$; therefore $z \in [-\delta, \delta]$.

The motion of the state variable y is dominated by Eq (8):

$$\ddot{y} = f_r(\mu e^{-y/\sigma} - 1) + f_r(\beta {v_r}^2 \sqrt{1 - \frac{y}{y_\infty}} e^{-y/\sigma} - \gamma |v_r| \dot{y} e^{-y/\sigma}) \tag{8}$$

In Eq (8): $\beta > 0$, $\gamma > 0$ are free parameters. The first term on the right side of Eq (8) becomes from the asperity shape in the normal direction, and the second term is the normal component of the force generated by the collision of the asperities.

When the displacement difference $|x_1 - x_i| = d$, the system collides. Since the nonlinear system contains collision and friction, the motion state of the system will be converted between chatter, sticking and collision. In order to more fully understand the changes in the motion process of the system, according to the force and velocity changes of the mass 1, the motion process of the system is divided into the following situations.

Case 1: Mass M_1 moves under the action of harmonic excitation force $F\,cos(\Omega T + \varphi)$, and the system force analysis of mass M_1 is carried out. Let f_1 represent the resultant force of mass M_1, the $f_1 = f cos(\omega t + \varphi) - \xi_1 \dot{x}_1 - k_1 x_1 - \varepsilon k_1 x_1^3 + k_2 x_2 + \varepsilon k_2 x_2^3 + k_3 x_3 + \varepsilon k_3 x_3^3 + \xi_2[1 + \eta sgn(\dot{x}_2 - \dot{x}_1)](\dot{x}_2 - \dot{x}_1)^{1/3} + \xi_3[1 + \eta sgn(\dot{x}_3 - \dot{x}_1)](\dot{x}_3 - \dot{x}_1)^{1/3}$. When the difference between the motion displacement of the mass M_1 and the mass M_2 or the mass M_3 is equal to gap d, the system collides, due to the symmetry of the left wedge and the right wedge, the resultant force on mass M_1 is the resultant force in the vertical direction as shown in the Figure 3, and the judgment expression is:

$$|x_1 - x_i| = d \qquad (i = 2, 3) \tag{9}$$

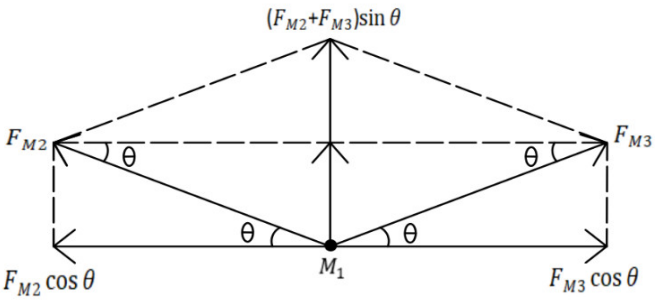

Figure 3. Collision force composite diagram.

According to the law of conservation of momentum and the relationship between the velocity before and after the collision, it can be obtained that:

$$\begin{cases}\mu_m\dot{x}_{1+}+\dot{x}_{i+}=\mu_m\dot{x}_{1-}+\dot{x}_{i-}\\ \dot{x}_{i+}-\dot{x}_{1+}=-R(\dot{x}_{i-}-\dot{x}_{1-})\end{cases}\quad (i=2,3) \tag{10}$$

Among them, R is the collision recovery coefficient.

Case 2: If the resultant force of the mass M_1 is greater than zero or equal to zero and the relative velocity of mass M_1 and mass M_1 or M_1 is not zero, the mass M_1 performs accelerated slip motion, and then $f_1 \geq 0$, $|\dot{x}_1-\dot{x}_2| \neq 0$.

Case 3: If the resultant force of the mass M_1 is less than zero and the relative velocity of mass M_1 and mass M_1 or M_1 is not zero, the mass M_1 performs decelerated slip motion, and then $f_1 \leq 0$, $|\dot{x}_1-\dot{x}_2| \neq 0$.

Case 4: If the resultant force of mass M_1 is less than zero and the relative velocity between mass M_1 and mass M_2 or mass M_3 is zero, that is, $f_1 < 0$, $|\dot{x}_1-\dot{x}_2| = 0$, mass M_1 is in a sticking state.

Based on the above four cases, the numerical simulation of the wedge friction damper oblique collision system with gap and friction is carried out to analyze its dynamic behavior. In order to study the periodic motion and bifurcation characteristics of the wedge damper system, the Poincaré section $\sigma=\{(x_1,\ \dot{x}_1,\ x_i,\ \dot{x}_i,\ \theta)\in \mathrm{R}^4\times \mathrm{S},\ x_1-x_i=d,\ \dot{x}_1=\dot{x}_{1+},\ \dot{x}_i=\dot{x}_{i+}\}$ is selected.

The Poincare mapping is established:

$$X^{(j+1)}=\tilde{f}\left(v,X^{(j)}\right) \tag{11}$$

Of which:

$$X^{(j)}=\left[\tau^{(j)},X_i{}^{(j)},\dot{X}_{1+}^{(j)}\dot{X}_{i+}^{(j)}\right]^T$$

$$X^{(j+1)}=\left[\tau^{(j+1)},X_i{}^{(j+1)},\dot{X}_{1+}^{(j+1)},\dot{X}_{i+}^{(j+1)}\right]^T \tag{12}$$

In Eqs (11) and (12), $i=2,3, X\in \mathrm{R}^4$, v is a real parameter. The periodic motion in the following discussion is represented by n-p-q-l, where n represents the number of excitation periods, p represents the number of collisions, q represents the number of chatters, and l represents the number of stickings.

3. The influence of Dankowicz friction on the system

In advance, through a large number of data simulation experiments, we find the different dynamic behavior of the system under different parameters, and select the system parameters of the wedge friction damper combined with the engineering practice: M_1 = 489 kg, M_2 = 537.9 kg, F = 112 N, K_1 = 2.4 × 10^4 N/mm, K_2 = K_3 = 2.04 × 10^4 N/mm, C_1 = 171 N·s/m, C_2 = C_3= 643 N·s/m. Take the parameters into Eq (1), and calculate the dimensionless parameters of the system: k_1 = 0.8, k_2 = 0.85, k_3 = 0.85, m_2 = 1.1, m_3 = 1.1, R = 0.85, ξ_1 = 0.05, ξ_2 = 0.15, ξ_3 = 0.15, μ_m = 0.4, μ = 0.2, β = 100, y_∞ = 2000, δ = 0.0001, γ = 3000, σ = 0.01, α_1 = 2.2, f = 1, f_r = 0.2, θ = 53. Set the initial value: x_1 = 0, x_2 = 0, $\dot{x}_1$ = 0, $\dot{x}_2$ = 0. Taking the dimensionless frequency as the bifurcation control parameter, the global and local bifurcation diagrams of the system motion obtained by numerical simulation are shown in Figure 4. From the bifurcation diagram in Figure 4, it can be seen that as the frequency ω increases from 1 to 8, the system motion undergoes inverse periodic doubling

bifurcation, periodic doubling bifurcation, Grazing bifurcation, and Hopf bifurcation to each other between single-period, multi-period, quasi-period, and chaos. As shown in Figure 4(a), when $\omega \in [1, 1.454]$, the system is in a chaotic state, and when $\omega \in [1.454, 3.2]$, the system is in period three motion. As shown in Figure 4(b), when $\omega \in [3.2, 4.1]$, the system is in chaotic and multi-period motion. As shown in Figure 4(c), when $\omega \in [4.3, 4.66]$, the system is in period six motion and period nine motion successively, and then Hopf bifurcation occurs. When $\omega \in [4.66, 4.93]$, the system is in almost periodic motion. As shown in Figure 4(a), when [4.93, 6.33], the system transitions between periodic three motions, periodic six motions and periodic twelve motions. As shown in Figure 4(d), when [7, 8], the system transitions between multi-period motion and chaos. By analyzing the motion process of the system with frequency change, it is found that the system is a stable periodic motion in the parameter interval $\omega \in [1.75,3.24]$, $\omega \in [4.029,4.65]$, $\omega \in [5,6.33]$ and $\omega \in [6.6,7.225]$. The elastic force, damping force, and external excitation force are coupled to each other due to collision and friction in the motion system of the wedge shock absorber, which leads to chatter. Through the phase diagram, poincare section diagram, and time history diagram of the system motion with the change of bifurcation control parameters, the chatter, collision, and sticking of the wedge damper during the train operation are studied in detail.

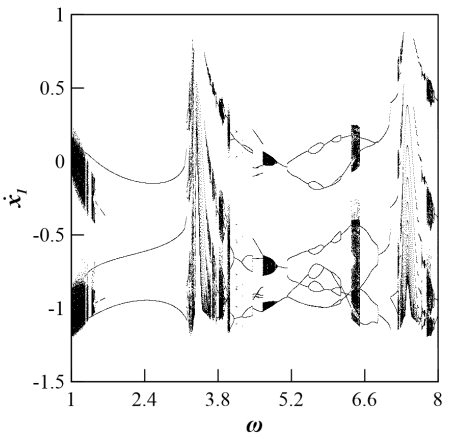

(a) Global bifurcation of system motion

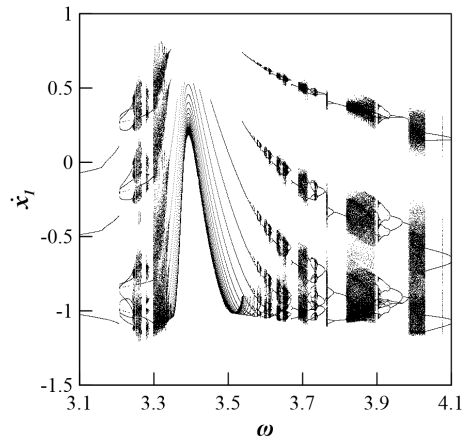

(b) Local bifurcation of system motion

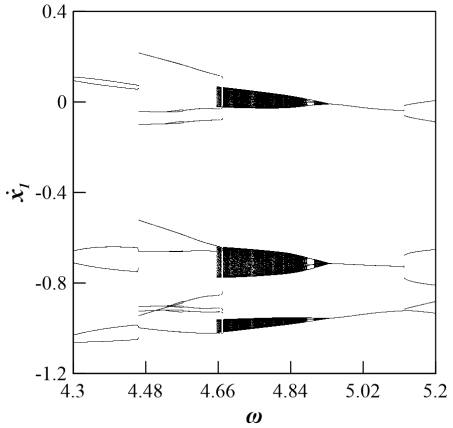

(c) Local bifurcation of system motion

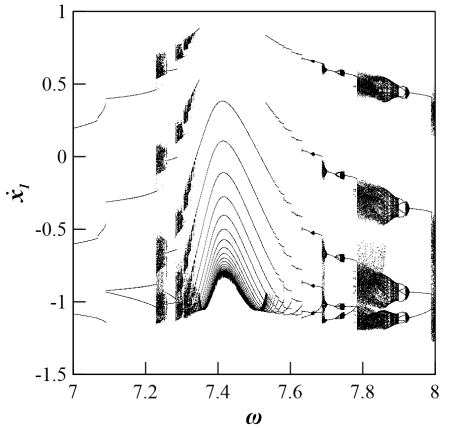

(d) Local bifurcation of system motion

Figure 4. System motion bifurcation diagram.

When the system frequency is $\omega = 1.75$, as shown in Figure 5(a),(b), the corresponding phase diagram and displacement-time history diagram of the system are in the 1-3-2-0 periodic motion. Under the action of an external excitation, the system has three collisions and two chatters. As the external excitation frequency of the system increases, the system undergoes a period-doubling bifurcation and transits to a short period of twelve motions. When the system frequency $\omega = 3.24$, as shown in phase diagram 5(c) and displacement-time history diagram 5(d), the system is in a 1-12-9-0 periodic motion. Under the action of an external excitation, the system undergoes twelve collisions and nine chatters. As the system frequency continues to increase, when $\omega \in [3.35, 3.55]$ is selected, the sticking phenomenon occurs, and the system motion state is converted between sticking and chatter. As shown in Figure 5(e)–(p), the amplitude of the system chatter first decreases from large to small, reaches the minimum value at $\omega = 3.395$, and then decreases from small to large. Furthermore, the duration of the sticking phenomenon first increases from less to the longest at $\omega = 3.395$, and then the phenomenon gradually weakens until it disappears. The excitation frequency $\omega = 3.922$ is selected, as shown in Figure 5(q),(r). The system is in a 1-8-6-0 periodic motion. Under the action of an external excitation, the system has eight collisions and six chatters. When the excitation frequency $\omega = 4.029$, it can be seen from Figure 5(s),(t) that the system has a Grazing bifurcation. Because the displacement difference between mass M_1 and mass M_2 and mass M_3 is exactly d, the direction of the resultant force of mass M_1 suddenly changes, and under the action of the resultant force, it moves away from mass M_2 and mass M_3. At this time, the system is in a 1-6-6-0 periodic motion. Under the action of an external excitation, the system has six collisions and six chatters.

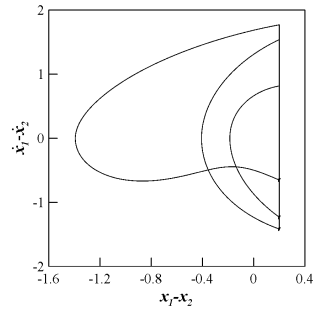

(a) Phase diagram ($\omega = 1.75$)

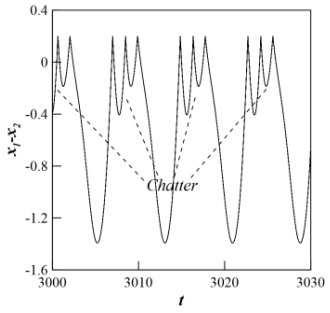

(b) Displacement-time history diagram

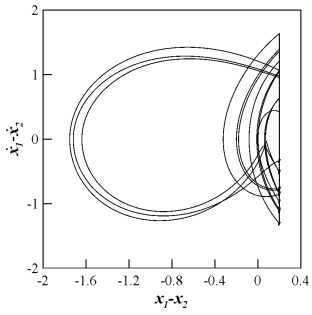

(c) Phase diagram ($\omega = 3.24$)

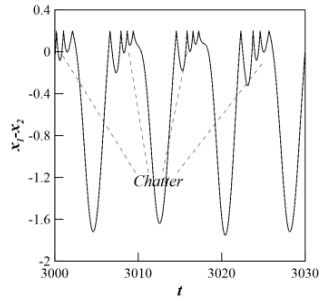

(d) Displacement-time history diagram

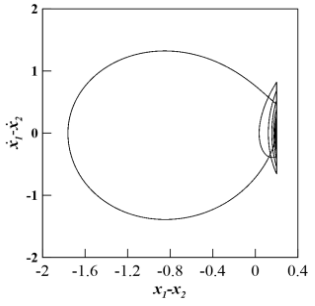

(e) Phase diagram ($\omega = 3.35$)

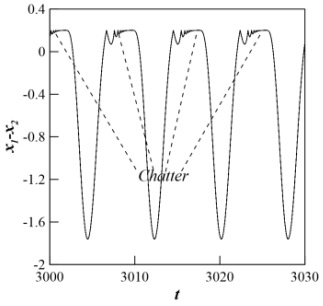

(f) Displacement-time history diagram

Continued on next page

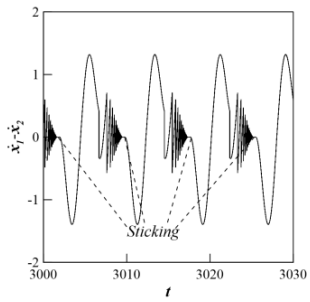

(g) Velocity-time history diagram

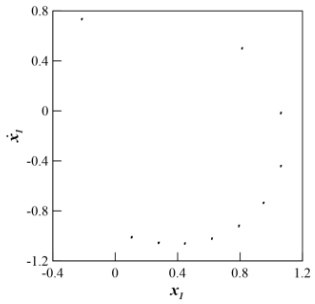

(h) Poincare cross section

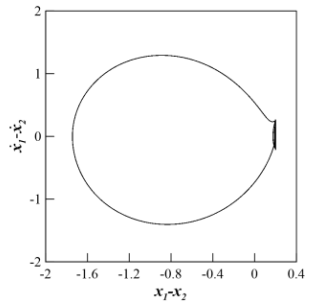

(i) Phase diagram ($\omega = 3.395$)

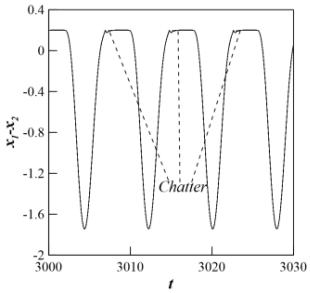

(j) Displacement-time history diagram

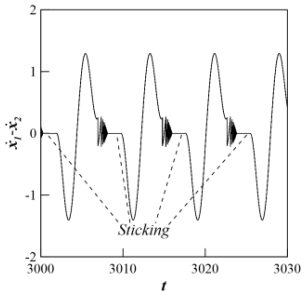

(k) Velocity-time history diagram

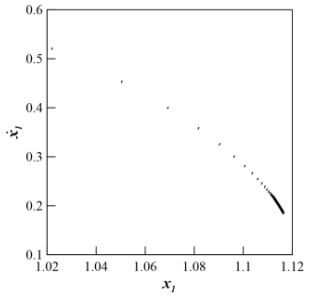

(l) Poincare cross section

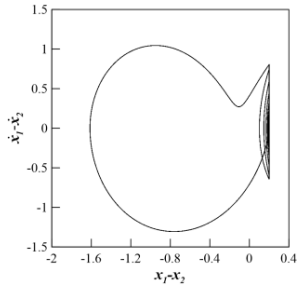

(m) Phase diagram ($\omega = 3.55$)

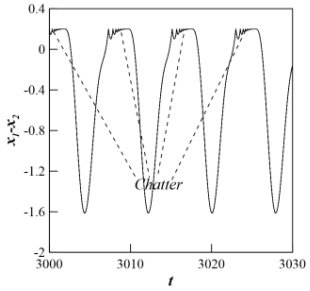

(n) Displacement-time history diagram

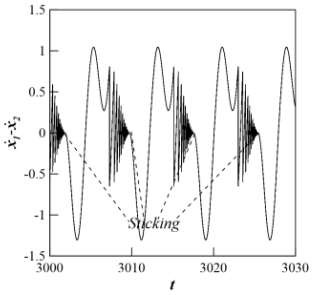

(o) Velocity-time history diagram

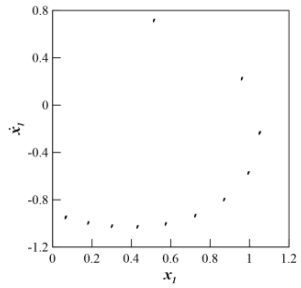

(p) Poincare cross section

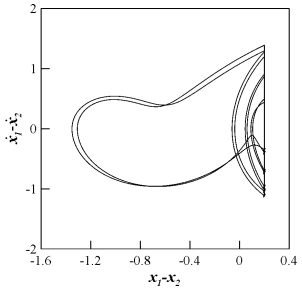

(q) Phase diagram ($\omega = 3.922$)

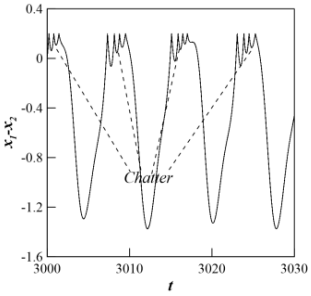

(r) Displacement-time history diagram

Continued on next page

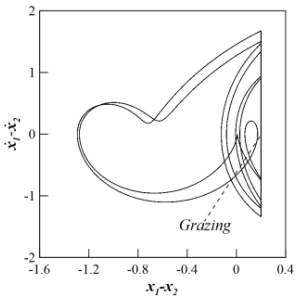

(s) Phase diagram ($\omega = 4.029$)

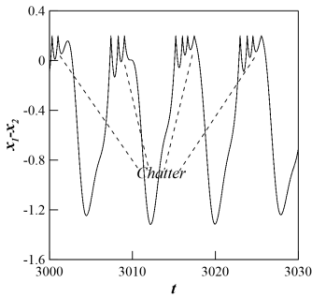

(t) Displacement-time history diagram

Figure 5. System motion diagram.

When the excitation frequency $\omega = 4.187$ is selected, as shown in Figure 6(a),(b), the corresponding phase diagram and displacement-time history diagram of the system are in the 1-3-3-0 periodic motion. Under the action of an external excitation, the system has three collisions and three chatters. Then, the system undergoes periodic doubling bifurcation, as shown in Figure 6(c)–(e). It can be seen that the system is in a 1-6-4-1 periodic motion. Under the action of an external excitation, the system undergoes six collisions, four chatters and one sticking. When the excitation frequency $\omega = 4.4258$, as shown in Figure 6(f)–(h), the system enters the period 1-9-7-2 motion, and the system appears the Grazing collision behavior through the Grazing bifurcation. When the excitation frequency $\omega \in [4.65, 4.9]$, as shown in Figure 6(i)–(l), with the increase of ω, the inverse Hopf bifurcation occurs in the system, and the system enters the periodic 1-3-2-1 motion through phase locking. Under the action of an external excitation, the system undergoes three collisions, two chatters and one sticking.

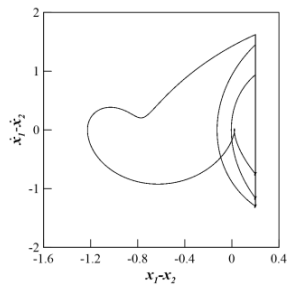

(a) Phase diagram ($\omega = 4.187$)

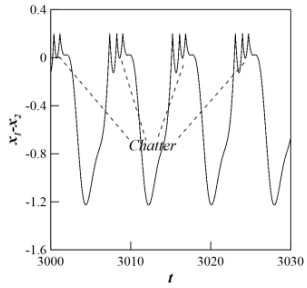

(b) Displacement-time history diagram

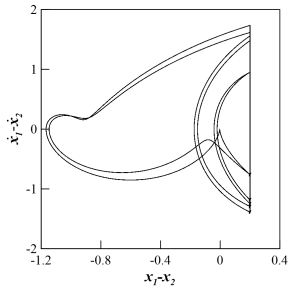

(c) Phase diagram ($\omega = 4.425$)

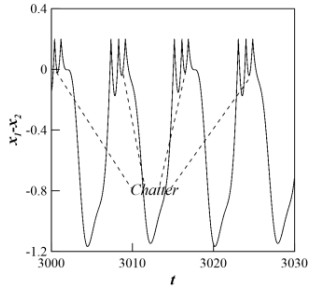

(d) Displacement-time history diagram

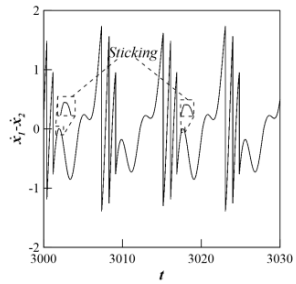

(e) Velocity-time history diagram

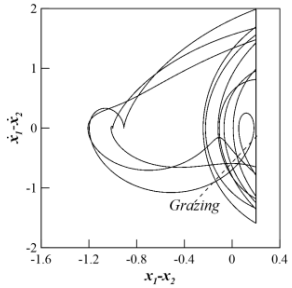

(f) Phase diagram ($\omega = 4.4258$)

Continued on next page

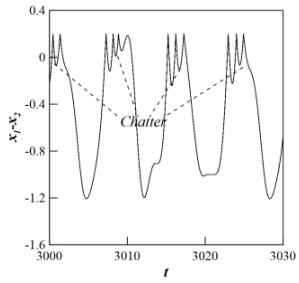

(g) Displacement-time history diagram

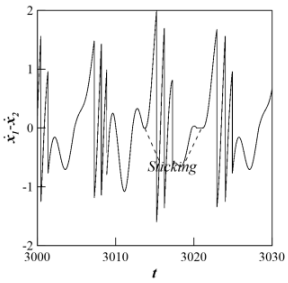

(h) Velocity-time history diagram

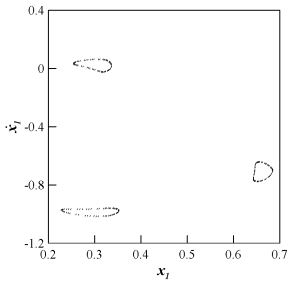

(i) Phase-lock ($\omega = 4.68$)

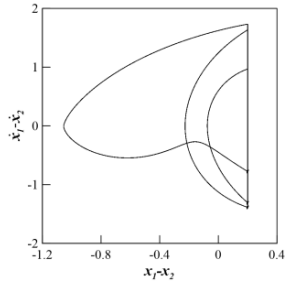

(j) Phase diagram ($\omega = 5$)

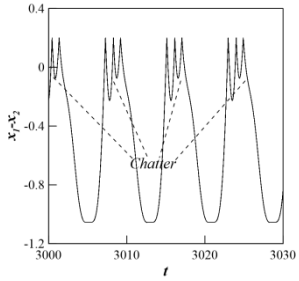

(k) Displacement-time history diagram

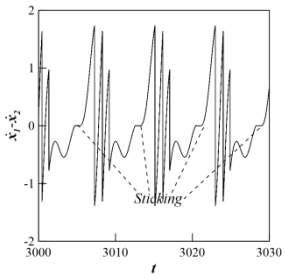

(l) Velocity-time history diagram

Figure 6. System motion diagram.

The excitation frequency $\omega = 6.12$ is selected, such as Figure 7(a)–(c), which shows that the system is in period 1-12-12-1 motion. Under the action of an external excitation, the system has twelve collisions, twelve chatters and one sticking. The excitation frequency $\omega = 6.34$ is selected, as shown in Figure 7(d),(e), which shows that the system enters the period 1-6-6-0 motion through the grazing bifurcation, and the sticking phenomenon disappears. Select the excitation frequency $\omega = 7.05$. As shown in Figure 7(f),(g), the system is in periodic 1-3-3-0 motion. Under the action of an external excitation, the system undergoes three collisions and three chatters. When the excitation frequency $\omega = 7.276$, the system enters the period 1-5-5-0 motion. Under the action of an external excitation, the system has five collisions and five chatters. As the system frequency continues to increase, when $\omega \in [7.34, 7.578]$ is selected, the system motion state is converted between sticking and chatter. As shown in Figure 7(e)–(p), the amplitude of the system chatter first decreases from large to small, reaches the minimum value at $\omega = 3.395$, and then decreases from small to large. At the same time, the duration of the sticking phenomenon increases from less to more, and the duration is the longest when $\omega = 3.395$, and then the phenomenon gradually weakens until it disappears. When the excitation frequency $\omega = 7.877$ is selected, the inverse Hopf bifurcation occurs in the system, and the chaotic state enters the periodic motion state through phase locking. When the excitation frequency $\omega = 7.905$, the system enters a period of 1-4-4-0 motion. Under the action of an external excitation, the system undergoes four collisions and four chatters.

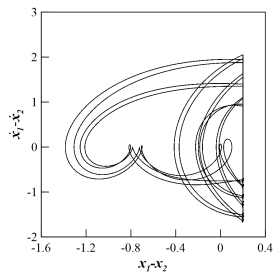

(a) Phase diagram ($\omega = 6.12$)

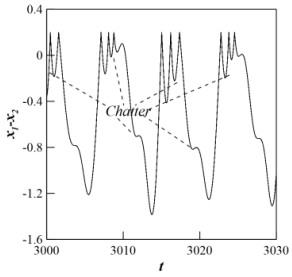

(b) Displacement-time history diagram

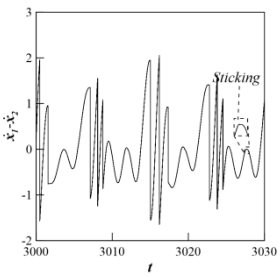

(c) Velocity-time history diagram

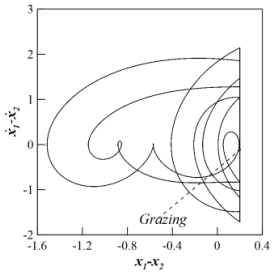

(d) Phase diagram ($\omega = 6.34$)

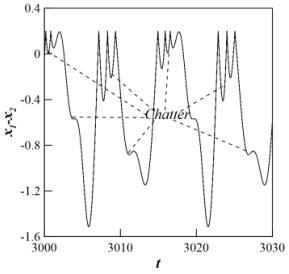

(e) Displacement-time history diagram

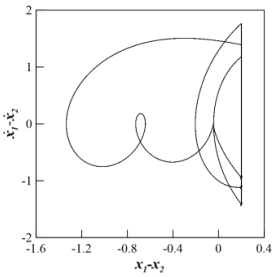

(f) Phase diagram ($\omega = 7.05$)

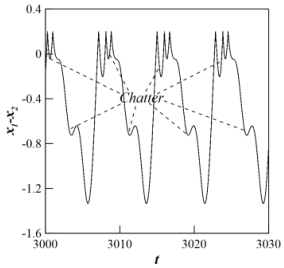

(g) Displacement-time history diagram

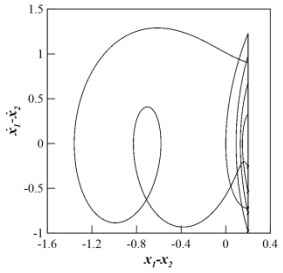

(h) Phase diagram ($\omega = 7.276$)

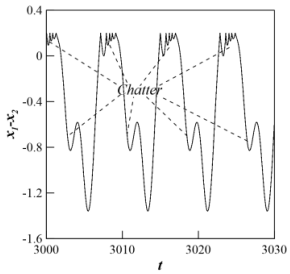

(i) Displacement-time history diagram

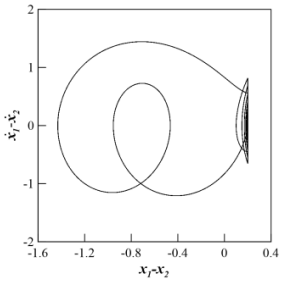

(j) Phase diagram ($\omega = 7.34$)

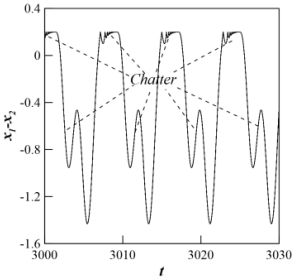

(k) Displacement-time history diagram

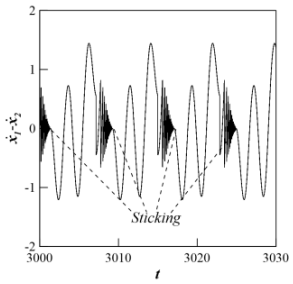

(l) Velocity-time history diagram

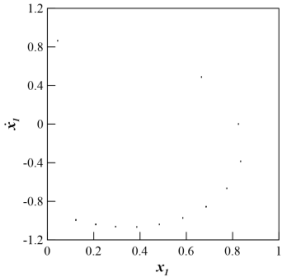

(m) Poincare cross section

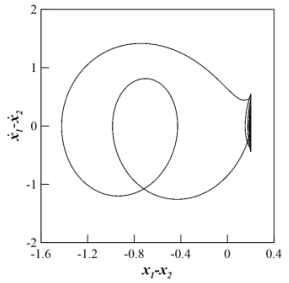

(n) Phase diagram ($\omega = 7.419$)

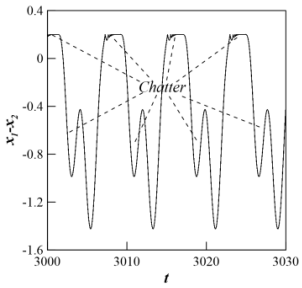

(o) Displacement-time history diagram

Continued on next page

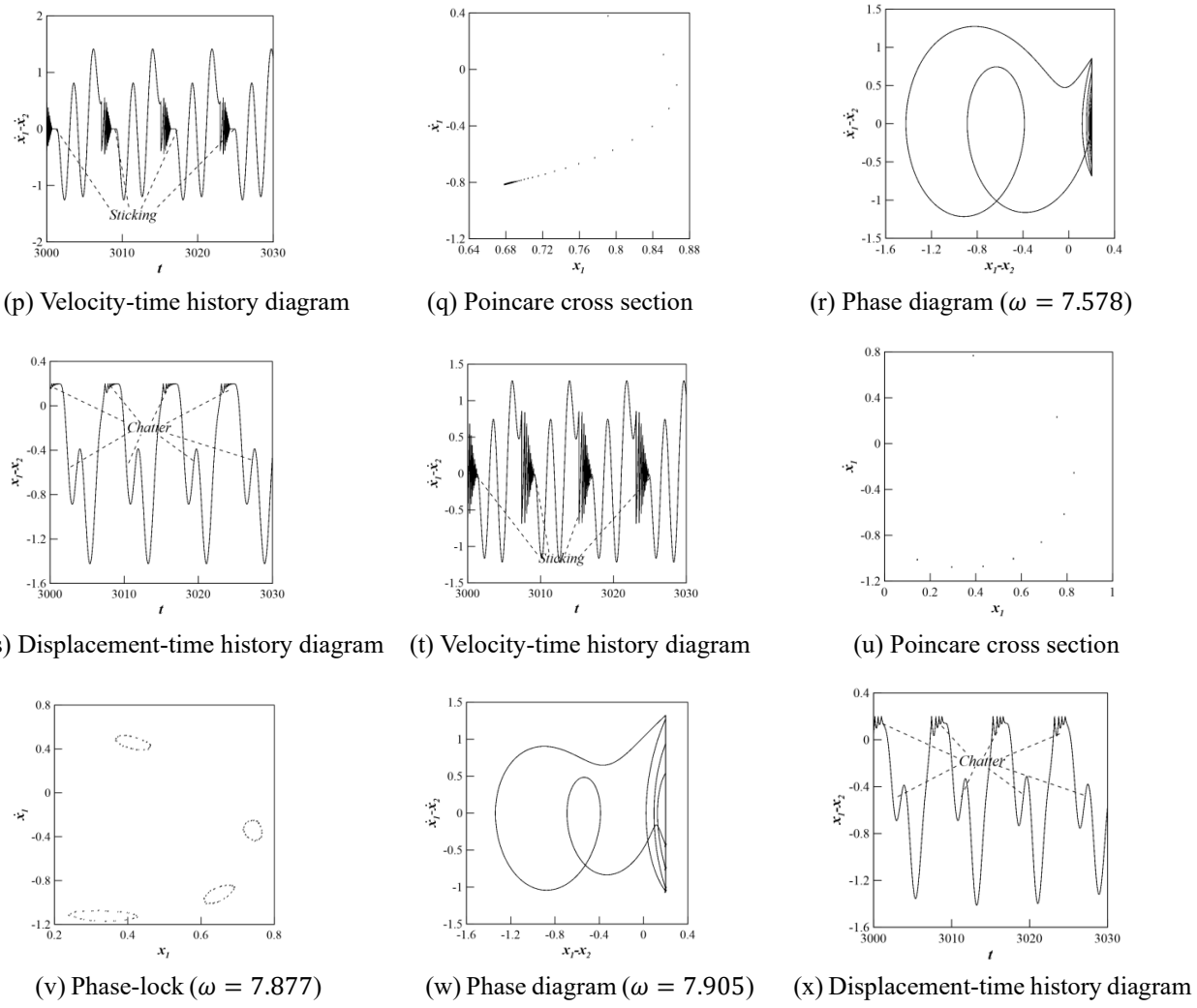

(p) Velocity-time history diagram (q) Poincare cross section (r) Phase diagram ($\omega = 7.578$)

(s) Displacement-time history diagram (t) Velocity-time history diagram (u) Poincare cross section

(v) Phase-lock ($\omega = 7.877$) (w) Phase diagram ($\omega = 7.905$) (x) Displacement-time history diagram

Figure 7. System motion diagram.

4. Effect of mass ratio on system motion

The change of the system motion transfer process and the parameter interval of the system stable motion is analyzed further. Through numerical simulation, it is found that the periodic bubble phenomenon of the system is very sensitive to parameter m_2, and the slight change of parameter m_2 makes the number of periodic bubbles of the system change or disappear. In order to better understand the influence of parameters on the dynamic behavior of the system, the system parameters $m_2 = 1.15$, $m_2 = 1.125$, $m_2 = 1.1$, $m_2 = 1.05$, $m_2 = 1$, $m_2 = 0.95$, $m_2 = 0.9$, $m_2 = 0.85$ are taken, and the remaining parameters remain unchanged. As the mass ratio decreases, when $m_2 \in [1.1, 1.15]$, as shown in Figure 8(a)–(c), the number of periodic bubble structures in the system increases from 4 to 7 and then to 11. When $m_2 \in [1, 1.05]$, as shown in Figure 8(d),(e), the periodic bubble structure disappears, and the system presents six chaotic bubble structures. When $m_2 \in [0.85, 0.95]$, as shown in Figure 8(f)–(h), the chaotic bubble structure disappears and the periodic bubble structure appears. The number of periodic bubble structures is 17, 6, and 3, respectively. Moreover, with the decrease of mass ratio, the transition region between flutter and viscosity of the system gradually moves to the left, and the period of period three motion window in the low frequency band is reduced. The Hopf

bifurcation phenomenon before the periodic bubble phenomenon or the chaotic bubble phenomenon gradually weakens until it disappears, and the window period of the periodic motion in the corresponding frequency band gradually increases.

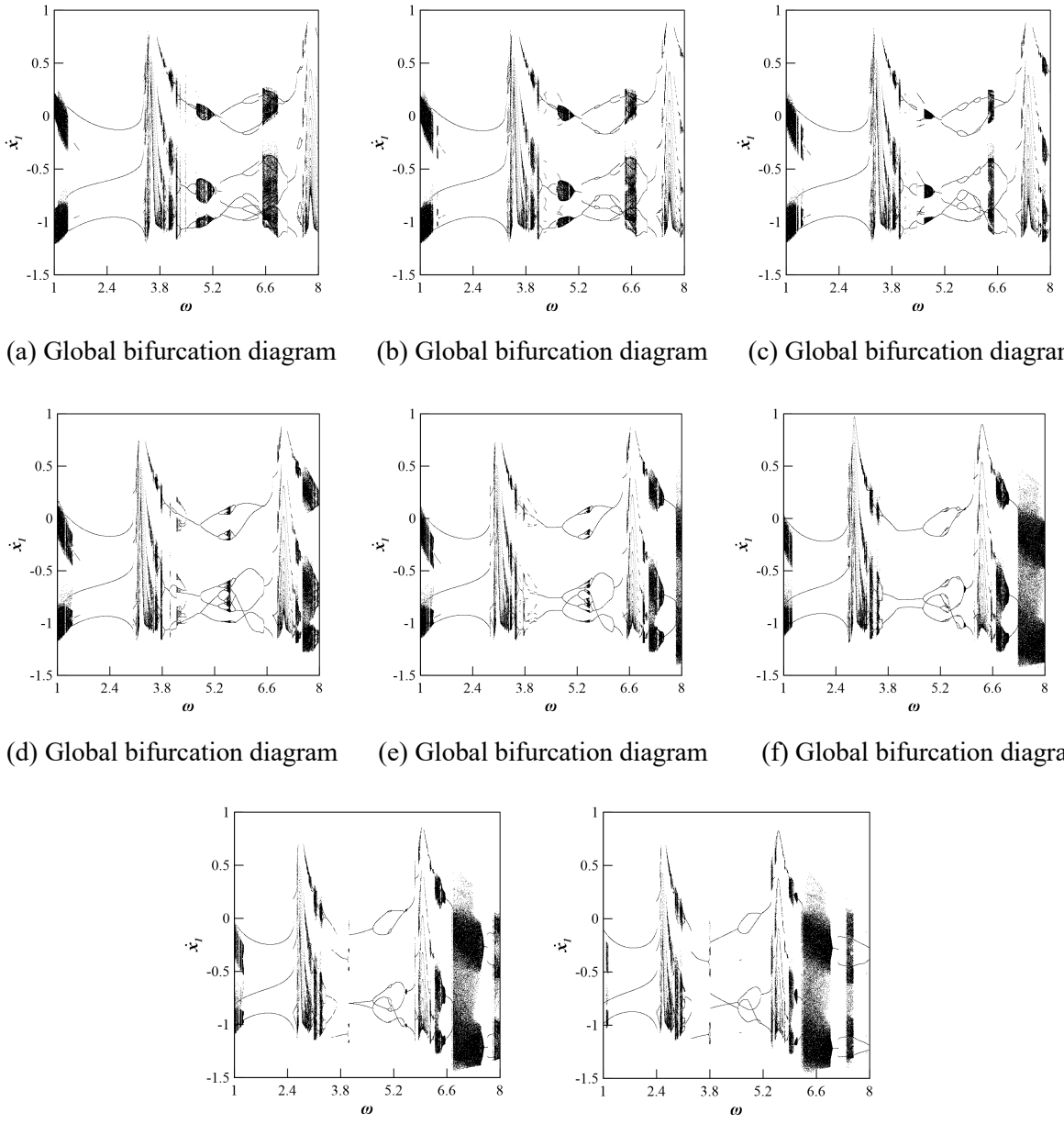

(a) Global bifurcation diagram (b) Global bifurcation diagram (c) Global bifurcation diagram

(d) Global bifurcation diagram (e) Global bifurcation diagram (f) Global bifurcation diagram

(g) Global bifurcation diagram (h) Global bifurcation diagram

Figure 8. Bifurcation diagram of system motion under different mass ratio parameters.

5. Conclusions

In this paper, the dynamic model of a kind of wedge damper with dynamic friction is simplified, and the differential equation of system motion is established. According to the change of mass force, the motion situation of the system and the judgment conditions of each situation are discussed. The dynamic characteristics of the system are analyzed by a large number of data simulation. The

simulation results show that:

Under certain parameters, with the change of excitation frequency, the system undergoes periodic doubling bifurcation, inverse periodic doubling bifurcation, Grazing bifurcation and Hopf bifurcation between single period, multi period, quasi period, and chaos. In addition, when the excitation frequency of the system is between [5.2, 6.1], there is a periodic bubble phenomenon in the system motion. When the excitation frequency of the system is between [3.35, 3.55], [4.425, 6.12], and [7.34, 7.758], there are chatter and sticking phenomena in the system motion. When the excitation frequency of the system is between [1.75, 3.24] and [3.92, 4.425], the sticking phenomenon disappears, and only the chatter phenomenon exists.

When other parameters remain unchanged, as the mass ratio decreases, the number of periodic bubble structures of the system motion increases exponentially, that is, the number of cycles of the system motion increases exponentially. Then, the periodic bubble structure disappears and the chaotic bubble structure appears. Finally, the chaotic bubble structure disappears and the system enters periodic motion.

Through the theoretical analysis and numerical simulation of the wedge friction damper oblique collision system with Dankowicz dynamic friction, it provides a certain reference basis for the selection of structural parameters and system motion process control of wedge friction damper for freight train bogies in practical engineering. Furthermore, the method of applying the bifurcation theory of mapping to study the stability, bifurcation, and chaos formation process of periodic motion of multi-degree-of-freedom impact vibration system can also be used to study the periodic motion, stability and bifurcation of other types of impact vibration systems, such as double-mass impact vibration molding machine, pile driver, vibration hammer, wheel-rail collision of high-speed train, etc., and can also be applied to the dynamic analysis of some mechanical systems with clearance and elastic constraints.

Use of AI tools declaration

The authors declare they have not used Artificial Intelligence (AI) tools in the creation of this article.

Acknowledgments

The work was supported by the Gansu Provincial Science and Technology Plan Project (21YF5WA060) and the National Natural Science Foundation of China (11302092). The author is grateful for the financial support.

Conflict of interest

The authors declare that there are no conflicts of interest.

References

1. J. Duan, Q. Ding, Dynamics and vibration reduction of oblique collision vibration of three masses (in Chinese), *J. Vib. Eng.*, **26** (2013), 68–74. https://doi.org/10.16385/j.cnki.issn.1004-4523.2013.01.002

2. L. Ling, M. Dhanasekar, D. P. Thambiratnam, Frontal collision of trains onto obliquely stuck road trucks at level crossings: derailment mechanisms and simulation, *Int. J. Impact Eng.*, **100** (2017), 154–165. https://doi.org/10.1016/j.ijimpeng.2016.11.002
3. M. J. Dong, Q. Ding, Study on vibration localization of oblique impact of whole-circle bladed disk with tips system (in Chinese), *J. Aerosp. Power*, **29** (2014), 2914–2923. https://doi.org/10.13224/j.cnki.jasp.2014.12.018
4. M. J. Wu, S. Y. Zhao, I. Azim, J. Zhu, X. H. Huang, A novel oblique impact model for elastic solids, *Int. J. Impact Eng.*, **180** (2023), 104699. https://doi.org/10.1016/j.ijimpeng.2023.104699
5. M. Ji, Y. Sekiguchi, K Inaba, M. Naito, C. Sato, Forward and inverse analysis of transient responses for a cantilevered rectangular plate under normal and oblique impact loadings, *Int. J. Impact Eng.*, **174** (2023), 104514. https://doi.org/10.1016/j.ijimpeng.2023.104514
6. J. P. Li, J. J. Fan, Discontinuous dynamics of a 3-DOF oblique-impact system with dry friction and single pendulum device, *Nonlinear Dyn.*, **111** (2023), 4977–5021. https://doi.org/10.1007/s11071-022-08062-6
7. R. H. Davis, J. W. Sitison, Oblique collisions of two wetted spheres, *Phys. Rev. Fluids*, **5** (2020), 054305. https://doi.org/10.1103/PhysRevFluids.5.054305
8. A. Kira, H. Hamashima, K. Hokamoto, M. Fujita, Numerical simulation of oblique collision of flier plate, *Mater. Sci. Forum*, **767** (2013), 192–195. https://doi.org/10.4028/www.scientific.net/MSF.767.192
9. Z. S. Liu, M. Zhang, G. H. Zhang, Z. X. Liu, Characteristics of impact-contact and friction between tips of blades based on LuGre model (in Chinese), *J. Vib. Shock*, **31** (2012), 172–178. https://doi.org/10.13465/j.cnki.jvs.2012.12.036
10. A. Saha, M. Wiercigroch, K. Jankowski, P. Wahi, A. Stefanski, Investigation of two different friction models from the perspective of friction-induced vibrations, *Tribol. Int.*, **90** (2015), 185–197. https://doi.org/10.1016/j.triboint.2015.04.029
11. Y. L. Zhang, B. B. Tang, L. Wang, S. S. Du, Dynamic analysis for a vibro-impact system with clearance under kinetic friction (in Chinese), *J. Vib. Shock*, **36** (2017), 58–63. https://doi.org/10.13465/j.cnki.jvs.2017.24.009
12. H. L. Li, F. Li, M. H. Fu, X. Yang, D. C. Zhang, Dynamic modeling and simulation of wedges friction damper (in Chinese), *J. Railway Sci. Eng.*, **12** (2015), 1191–1199. https://doi.org/10.19713/j.cnki.43-1423/u.2015.05.031
13. Y. W. Li, *Study on the Vibration Chatacteristics of 100t Load Heavy Haul Freight Car*, MA thesis, Southwest Jiaotong University, 2018.
14. Z. Y. Song, M. H. Fu, S. Chen, Effects of wedge friction angle on dynamic performance of three-angle bogie (in Chinese), *Mach. Build. Autom.*, **50** (2021), 62–66. https://doi.org/10.19344/j.cnki.issn1671-5276.2021.02.017
15. Z. M. Liu, Analysis and design suggestions on relative friction coefficient of freight car bogie, *Railway Locomot. Car*, **43** (2023), 122–127.
16. J. F. Shi, X. F. Gou, Y. L. Zhang, Erosion and bifurcation of the safe basin of a two-degree-of-freedom damping boring bar system (in Chinese), *J. Vib. Shock*, **37** (2018), 238–244. https://doi.org/10.13465/j.cnki.jvs.2018.22.036

17. Y. L. Zhang, C. Wei, L. Wang, Z. L. Wang, Dynamic analysis of the impact vibration system with Dankowicz dynamic friction, *Noise Vib. Control*, **41** (2021), 14–20. https://doi.org/10.3969/j.issn.1006-1355.2021.03.003

AIMS Press